The Impact of the Ionosphere on Interferometric SAR Processing

Franz J Meyer, Jeremy Nicoll
Alaska Satellite Facility (ASF)
University of Alaska Fairbanks
fmeyer@asf.alaska.edu

***Abstract*—The impact of ionospheric propagation effects on the signal properties of SAR systems is significant and increases with decreasing carrier frequency. Besides polarimetric applications, also interferometric SAR processing can be significantly affected. Relative range shifts, internal image deformations, range and azimuth blurring, and interferometric phase errors are the most significant effects to be considered. In this paper we provide the theoretical background for ionospheric effects on InSAR. We quantify expected magnitudes of the respective effects for various existing SAR sensors and discuss methods for their detection and correction. Real data examples, mainly stemming from the ALOS PALSAR mission, are presented to verify the derived theory.**

Keywords-polarimetric SAR calibration, ionospheric effects, SAR Interferometry, ionospheric phase screen.

I. INTRODUCTION

At L-band, the ionosphere is assumed to have considerable effects on synthetic aperture radar (SAR) image quality. Though ionospheric distortions of polarimetric SAR data have gained recent notoriety (see e.g. [1-3]), interferometric SAR processing can also be significantly affected by the ionosphere (see e.g. [4]). Relative range shifts between interferometric partners, internal image deformations, range and azimuth blurring, loss of coherence, and interferometric phase errors are the most significant effects to be considered.

In this paper we will provide the theoretical background for ionospheric effects on InSAR and will quantify expected magnitudes of the respective effects for various existing SAR sensors. Methods for detecting and correcting ionospheric effects on InSAR, and for recovering the optimal interferogram quality are discussed. By analyzing the vast ALOS PALSAR archive at the Alaska Satellite Facility (ASF), the probability of occurrence of ionospheric effects in InSAR data is determined in both space and time. Weaknesses of the derived methods as well as unresolved issues are discussed. The consequences of previous findings for future satellite missions are mentioned. A description of future work concludes the paper.

II. IONOSPHERIC EFFECTS ON SAR INTERFEROMETRY

The effect of the ionosphere on traversing microwave signals is defined by its refractivity and can be approximated by

$$N_{iono} = (n_{iono} - 1)\cdot 10^6 \approx -K \cdot 10^6 \frac{n_e}{{f_0}^2} \quad (1)$$

where n_{iono} is the ionospheric refraction index, $K = 40.28\,(m^3/s^2)$, n_e is the density of free electrons in the ionosphere, and f_0 is the frequency of the traversing signal. As seen from Equation (1), ionospheric effects are strongly dependent on the solar activity (defines n_e) and the frequency of observation and increase with lower frequencies.

For a hypothesized nadir-looking radar, the two-way ionospheric phase shift of frequency f can be derived from (1) and given by

$$\phi(f) = -2\pi f \frac{2}{10^6}\int_0^H \frac{N_{iono}(f,h)}{c}dh \approx 2\pi\frac{2K}{cf}TEC \quad (2)$$

With c the vacuum speed of light and TEC being the column density of free electrons integrated along the vertical.

From (2) , the phase delay

$$\tau_{ph} = -\frac{\phi(f_0)}{2\pi f_0} \approx -\frac{2K}{cf_0^2}TEC \quad (3)$$

and the group delay

$$\tau_{gr} = -\frac{1}{2\pi}\frac{d\phi(f)}{df}\bigg|_{f=f_0} \approx \frac{2K}{cf_0^2}TEC \quad (4)$$

at radar center frequency f_0 can be derived. Equations (3) and (4) can be readily transformed into range delays by multiplication with 2/c. For a typical non-nadir looking SAR, these equations must be multiplied by a geometry-dependent factor *M* to map from vertical to slant columns.

Note that the phase delay is negative. It describes the "advance" of the "phase" of the radar carrier. The (positive) group delay corresponds to the "delay" of the "envelope" of the (range-compressed) radar signal. Note that from (3) and (4), $\tau_{gr} \approx -\tau_{ph}$. Based on this information the effects of the ionosphere on InSAR can be developed.

A. Range and Azimuth Blurring

1) Range Blurring

Range blurring is a direct consequence of the non-linear frequency dependence of the ionospheric refraction index

causing a non-linear residual phase function $\delta\phi_r(f)$ across the range bandwidth. $\delta\phi_r(f)$ is approximately quadratic and can be described by

$$\delta\phi_r(f) \approx \frac{4\pi}{c_0}\frac{K}{f_0^3} TEC(f - f_0)^2 \quad (5)$$

If not considered during focusing, $\delta\phi_r(f)$ will cause range blurring in low-frequency SAR images of high bandwidth. For systems such as ALOS PALSAR, $\delta\phi_r(f)$ is expected to be significantly less than 5º and range blurring will be negligible.

2) Azimuth Blurring

Small scale turbulence in the ionosphere may cause high order phase fluctuations across the synthetic aperture causing a decrease in image resolution in azimuth. Turbulence phenomena at spatial scales below 10km however are assumed to be very rare and of low energy. Consequently, the effects on existing spaceborne SARs are considered to be insignificant.

B. Internal Image Deformations

Inhomogeneities of medium spatial wavelengths cause 'phase gradients' across the azimuth chirp, which result in an azimuth shift of objects in the focused image. These effects, which are dubbed 'azimuth streaks,' were originally reported in [5].

To determine the sensitivity of an ALOS PALSAR-like SAR system to TEC fluctuations of medium spatial extent, we assume a Gaussian TEC anomaly. To develop an anomaly model that matches typical ionospheric fluctuations, we considered observations of azimuth streaks published in [5]. According to these observations, a typical anomaly may have an amplitude of about 0.3 TECU and a width of 5 km. A schematic sketch of the simulated ionospheric anomaly and the associated azimuth shift, calculated for our reference system, is shown in Fig. 1. The shift reaches up to ±20 m.

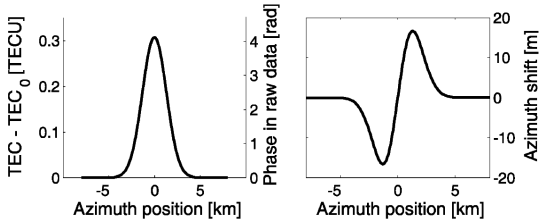

Figure 1. Simulated ionospheric anomaly associated with its corresponding azimuth shift.

C. Interferometric Phase Screen

According to Equation (2), lateral variations of TEC within a SAR image cause range delay and phase delay fluctuations. These fluctuations cause ionosphere induced phase screens that affect SAR Interferometry. Figure 2 shows a simulation of ionospheric phase screens in a wide swath L-band SAR image during spatially constant ionospheric conditions. Fig. 2(a) adresses the incidence angle-dependent ionospheric path delay assuming a 250-km-wide swath for two different ionospheric conditions. The differential phase delay between two acquisitions with ionospheric states of 20 and 40 TECU, respectively, gives rise to a residual phase ramp in range for an interferogram formed from these two images [see Fig. 2(b)]

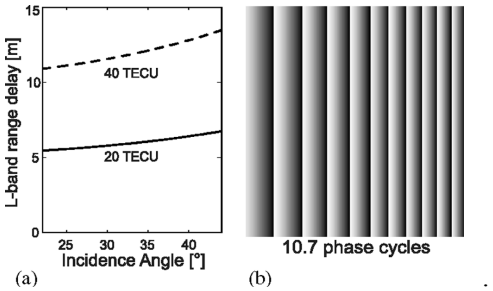

Figure 2. Simulated ionospheric anomaly associated with its corresponding azimuth shift.

D. Faraday Rotation and Associated Decorrelation

A simplified equation for Faraday rotation is

$$\Omega = \left(K/f^2\right) B\cos(\theta)\sec(\varphi)TEC \quad (6)$$

where Ω is the one-way Faraday rotation, B is the local geomagnetic field, f is the radio center frequency, θ is the angle between the magnetic field and the SAR pointing vector, φ is the incidence angle of the system, TEC is the total electron content, and K is a composite constant [6]. Equation (6) is based on the assumption that the magnetic field and electron density are constant and fixed at 350 km elevation.

From Equation (6) you can see that high TEC values alone are not sufficient to create strong Faraday rotation (FR); the orientation of the observation direction w.r.t. the magnetic field lines is another important factor. At the geomagnetic equator, where the line-of-sight of the radar sensor is almost perpendicular to the magnetic field, FR will stay low, even during strong ionospheric activity. Largest FR values are expected in mid-latitudes where TEC is still high, and θ is more favorable. Figure 3 exemplifies this latitude dependence based on predicted FR values for ALOS data holdings in the American ALOS Data Node (AADN) as of January 23, 2007.

Due to polarization differences between interferometric partners observed with different Ω, FR may cause decorrelation in SAR interferograms. Considering L-band HH signals, this decorrelation is small for $\Delta\Omega \le 30^\circ$ but increases markedly for larger angles. According to [4] and assuming negligible temporal decorrelation, a FR difference of $\Delta\Omega \approx 40^\circ$ would reduce coherence in an L-band HH interferogram to about 0.6. The reduction of coherence is dependent on the surface type causing strong correlation differences for different surface patches in the case of $\Delta\Omega$ close to 90º. In this case, high correlation may be observed in nonforested areas, and low correlation in forested regions.

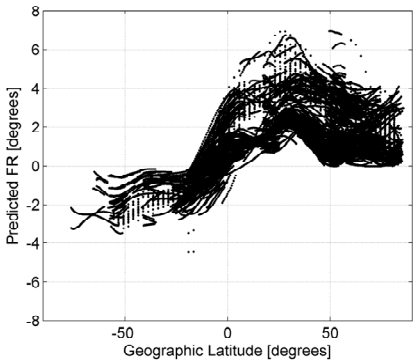

Figure 3. Predicted FR as a function of latitude. Data shown are for all ALOS PALSAR holdings at AADN as of January 23, 2007. Predicted values are calculated using Equation (6).

III. Measuring Ionospheric Effects from SAR

A. Measuring Faraday Rotation

The most commonly used approach for detecting FR in full-polarimetric SAR data was introduced in [10]. There the calibrated scattering matrix M' is transformed to a circular basis Z via

$$\begin{bmatrix} Z_{11} & Z_{12} \\ Z_{21} & Z_{22} \end{bmatrix} = \begin{bmatrix} 1 & j \\ j & 1 \end{bmatrix} \cdot \begin{bmatrix} M'_{hh} & M'_{vh} \\ M'_{hv} & M'_{vv} \end{bmatrix} \cdot \begin{bmatrix} 1 & j \\ j & 1 \end{bmatrix} \quad (7)$$

From Equation (7), an estimate for Ω can be derived by calculating

$$\hat{\Omega} = \frac{1}{4}\arg\left(Z_{12}Z_{21}^{*}\right). \quad (8)$$

Other approaches for estimating FR from full-pol SAR data are published in [4] and [9]. However, they are reported to be more sensitive to residual calibration errors and uncompensated system noise.

For the FR estimation algorithm of Equation (8), remaining calibration errors cause target dependent biases in $\hat{\Omega}$. In a worst-case scenario, this bias may be as much as 3º, however, biases in the order of 1º are more likely to occur. Also, the FR bias is *dependent on the magnitude* of the unbiased (true) Faraday rotation in a non-linear fashion and generally *increases with* Ω. As the bias is dependent on the target type, FR estimates may vary within a SAR image by up to 1.5º, causing a spread of the statistical distribution of measured FR.

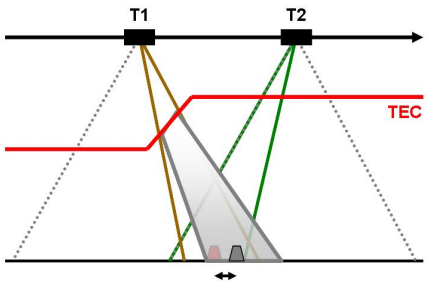

Figure 4. Origin of differential azimuth shifts between SAR sub-look images subject to ionospheric turbulence.

B. Detecting Internal Deformations

An image-by-image method for estimating internal image deformations is based on sub-look processing. Two non-overlapping sub-looks are extracted from the original SAR azimuth spectrum and two images are formed. Due to the correspondence of azimuth frequency and SAR look direction, a high frequency sub-look corresponds to an image observed in forward looking geometry, while a low frequency sub-look represents a backward looking image. As the sub-look images observe the same object on ground from slightly different locations along the orbit (compare Figure 4) they 'see' through different parts of the ionosphere. A difference in the ionospheric gradients at these locations results in relative shifts between the images, which can be detected by cross-correlation methods. As the looks are spectrally independent, complex cross-correlation methods are not applicable and less robust amplitude correlation is required.

Examples of high resolution shift maps derived from sub-look images are presented in Figure 5. The shift maps correspond to the second derivative of the TEC during the time of data acquisition. Relative shifts of up to 15 pixels have been observed, corresponding to about 130m differential shift on ground. Because of the observation geometry of SAR, the range extension of the observed ionospheric volume is very narrow. Therefore, the shift pattern in most of the examples is aligned in cross-track direction. By double integration of the shift maps in azimuth direction, high resolution maps of ionospheric variations along the image can be derived. Such maps contain valuable information for both SAR quality analysis and studies of small scale ionospheric turbulences.

IV. Derivation of Phase Delay Maps from FR Measurements

A. Background

Faraday rotation measurements can be used in combination with the model in Equation (6) to derive phase delay maps if knowledge about the observation geometry and the geomagnetic field are available. The geomagnetic field used

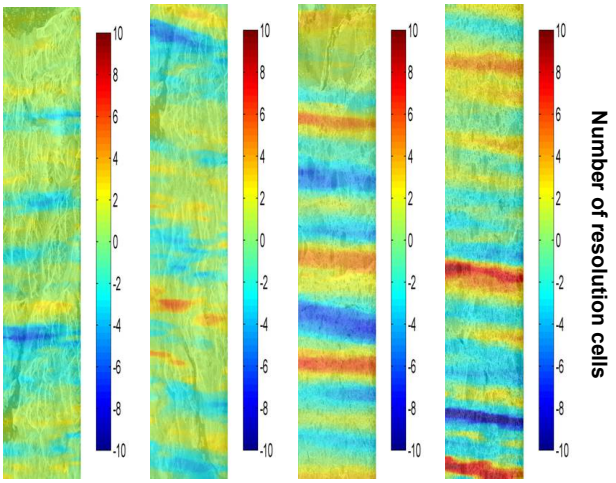

Figure 5. Estimated azimuthal shifts in between SAR sub-looks subject to ionospheric turbulence for four different PALSAR frames.

for the derivation of phase delay maps was calculated from geomagnetic data provided by the National Geophysical Data Center (http://www.ngdc.noaa.gov/), based on the International Geomagnetic Reference Field. If phase delay maps can be derived with sufficient accuracy, they are a useful tool for correcting ionospheric influences on the interferometric phase.

Two examples of ionospheric phase screens together with their corresponding Faraday rotation maps are shown in Figure 6. In these examples strong small-scale ionospheric turbulences are present raising the Faraday rotation locally by several degrees. Consequently, the phase delay maps show severe phase distortions. Due to the narrow swath of full-pol PALSAR data, no significant range dependent phase ramps are evident.

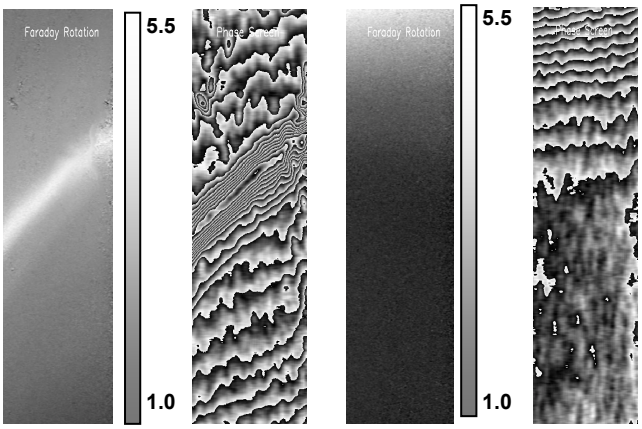

Figure 6. FR map estimated from full-pol PALSAR data and derived phase delay map for the area of Gakona, Alaska. A strong small scale ionospheric event is present in the data.

B. Precision of Phase Delay Maps

To determine the benefit of ionospheric phase delay maps for Interferometry, their precision has to be analyzed. The two major contributors to variance in the phase delay determination are errors in Faraday rotation measurements $\hat{\sigma}_\Omega$ and uncertainties in the geomagnetic field σ_B. From experience, the standard deviation of FR measurements from full-pol PALSAR images is fairly constant from image to image, and is assumed to be $\hat{\sigma}_\Omega = 0.25^\circ$. The standard deviation of the components of the geomagnetic field is specified to be about 250 nanoTesla [11]. Errors in the geomagnetic field and FR were propagated to error in phase cycles from the root sum square of their relative variances. Figure 7 shows the estimated standard deviation of phase delay measurements σ_ϕ in wavenumbers for PALSAR data in ASF's AADN archive. Note that for geomagnetic latitudes outside of 20° north or south, errors are less than one phase cycle, but increase dramatically as location moves to the equator. This dramatic increase in error is due to the SAR's observation direction being almost orthogonal to the geomagnetic field and FR approaches zero even for large TEC values. In this case, errors in FR scale up to large errors in ϕ.

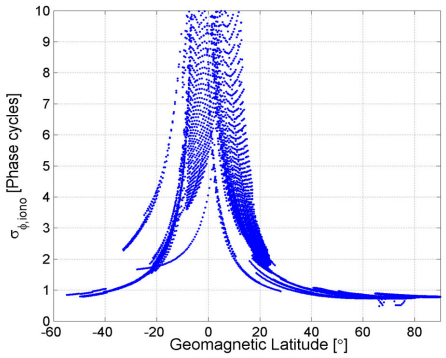

Figure 7. Standard deviation of phase delay maps derived from FR as a function of geomagnetic latitude for PALSAR data in the AADN archive.

V. Summary & Conclusions

The ionosphere may affect SAR Interferometry by introducing loss of coherence, internal image deformations, and phase distortions. Due to low to moderate FR during the lifetime of PALSAR, ionosphere induced coherence loss is assumed to be insignificant. Statistical analyses of internal image deformations indicate that, at this stage of the PALSAR mission, this effect is rare and occurs mainly in the polar regions. If full-polarimetric data is available, phase delay can be determined/predicted with an accuracy of less than one phase cycle for areas outside of ±20° geomagnetic latitude.

References

[1] A.R. Thompson, J.M. Moran, and G.W. Swenson, "Interferometry and Synthesis in Radar Astronomy," New York: Wiley, 1986.

[2] Z.-W. Xu, J. Wu, and Z.-S. Wu, "A Survey of Ionospheric Effects on Space-based Radar," Waves in Random Media, vol. 14, pp. 189–273, 2004.

[3] F. Meyer, R. Bamler, N. Jakowski, and T. Fritz, "The Potential of Low-Frequency SAR Systems for Mapping Ionospheric TEC Distributions," Geoscience and Remote Sensing Letters, vol. 2, no. 4, pp. 560–564, 2006.

[4] A. Freeman, and S. Saatchi, "On the Detection of Faraday Rotation in Linearly Polarized L-Band SAR Backscatter Signatures," Trans. On Geoscience and Remote Sensing, vol. 42, No. 8, pp. 1607–1616, 2004.

[5] A. Gray, K. Mattar, and G. Sofko, "Influence of ionospheric electron density fluctuations on satellite radar interferometry," Geophys. Res. Lett., vol. 27, no. 10, pp. 1451–1454, May 2000.

[6] P.A. Wright, S. Quegan, N.S. Wheadon, and C.D. Hall, "Faraday Rotation Effects on L-Band Spaceborne SAR Data," Trans. On Geoscience and Remote Sensing, vol. 41, No. 12, pp. 2735-2744, 2003.

[7] McLean, S., S. Macmillan, S. Maus, V. Lesur, A. Thomson, and D. Dater, December 2004, The US/UK World Magnetic Model for 2005-2010, NOAA Technical Report NESDIS/NGDC-1.

[8] Schaer, S.: Mapping and Predicting the Earth's Ionosphere using the Global Positioning System, Geodätisch- geophysikalische Arbeiten der Schweiz, Vol. 59, 1999.

[9] A. Freeman, "Calibration of Linearly Polarized Polarimetric SAR Data Subject to Faraday Rotation," Trans. On Geoscience and Remote Sensing, vol. 42, No. 8, pp. 1617–1624, 2004.

[10] S. H. Bickel and R. H. T. Bates, "Effects of magneto-ionic propagation on the polarization scattering matrix," Proc. IRE, vol. 53, pp. 1089–1091, 1965.

[11] McLean, S., S. Macmillan, S. Maus, V. Lesur, A. Thomson, and D. Dater, December 2004, The US/UK World Magnetic Model for 2005-2010, NOAA Technical Report NESDIS/NGDC-1.